




Enhanced electro active properties of NiCo₂O₄ nanostructures using garlic extract for the sensitive and selective enzyme-free detection of ascorbic acid

Abdul Ghaffar Solangi¹, Aneela Tahira¹, Abdul Sattar Chang², Tajnees Pirzada¹, Zulfiquar Ali Solangi¹⁰, Fouzia Chang², Muhammad Ali Bhatti⁸, Adeel Liaquat Bhatti¹¹, Shusheel Kumar¹¹, Abdul Hanan⁹, Elmuez Dawi³, Abd Al Karim Haj Ismail³, Shymaa S. Medany⁶, Ayman Nafady⁴, L. V. Kangle⁷, Brigitte Vigolo⁵, and Zafar Hussain Ibupoto^{2,*} 

¹Institute of Chemistry, Shah Abdul Latif University Khairpur Mirs, Sindh, Pakistan

²Dr. M.A Kazi Institute of Chemistry, University of Sindh, Jamshoro 76080, Pakistan

³Nonlinear Dynamics Research Centre (NDRC), Ajman University, P.O. Box 346, Ajman, United Arab Emirates

⁴Department of Chemistry, College of Science, King Saud University, Riyadh 11451, Saudi Arabia

⁵Université de Lorraine, CNRS, IJL, 54000 Nancy, France

⁶Department of Chemistry, Faculty of Science, Cairo University, Cairo, Egypt

⁷College of Resource and Environment, South-Central Minzu University, Wuhan 430074, China

⁸Institute of Environmental Sciences, University of Sindh Jamshoro, Jamshoro 76080, Sindh, Pakistan

⁹Key Laboratory of Superlight Material and Surface Technology, Ministry of Education, College of Materials Science and Chemical Engineering, Harbin Engineering University, 150001 Harbin, People's Republic of China

¹⁰Department of Chemical Engineering, Mehran University of Engineering and Technology, Jamshoro 7680, Sindh, Pakistan

¹¹Institute of Physics, University of Sindh Jamshoro, Jamshoro 76080, Sindh, Pakistan

Received: 12 May 2023

Accepted: 1 July 2023

Published online:
19 July 2023

© The Author(s), under exclusive licence to Springer Science+Business Media, LLC, part of Springer Nature 2023

ABSTRACT

Electroactive materials with low costs, simplicity, eco-friendliness, and efficiency are highly desirable for a variety of applications, including energy conversion, energy storage, and non-enzymatic sensing. Through the use of garlic green leaf biomass, active molecules are extracted to enhance NiCo₂O₄ nanostructure electroactive properties via reducing, stabilizing, and capping agents. A NiCo₂O₄ nanostructure electroactive material was created using 5 mL, 10 mL, and 15 mL of garlic leaf extract heated hydrothermally. An evaluation of the material's morphology, crystallinity, and surface chemical composition, as well as the application of electrochemical tests aimed at detecting ascorbic acid (AA) without the use of enzymes in phosphate buffer solution with pH of 7.4. Pure NiCo₂O₄ has the morphology of nanorods which was transformed into thinner nanowires consisting of nanoparticles with the addition of garlic leaves extract. Biosensors without enzymes have the advantages of being easy to make, reproducible, and stable over those with enzymes. NiCo₂O₄ nanostructures

Address correspondence to E-mail: zaffar.ibhupoto@usindh.edu.pk

<https://doi.org/10.1007/s10854-023-10937-2>

 Springer

fabricated with garlic leaf extract in a 10 mL volume are being developed as non-enzymatic AA sensors. The AA sensor presented here operates linearly from 0.5 to 8.5 mM with a detection limit of 0.01 mM. It was found that an AA sensor is highly selective, stable, repeatable, and capable of quantifying AA concentrations in various real-life samples.

1 Introduction

Ascorbic acid (AA) is a micronutrient that is essential for organism metabolism and growth. Additionally, it can be used to treat diseases like scurvy, poisoning, and atherosclerosis [1–3]. AA cannot be synthesized by the human body, so it must be consumed through food, vitamin supplements, and beverages containing vitamin C from outside sources. To diagnose diseases, detect illnesses, and promote health, the AA content of biological samples, food, and medications should be monitored to assist in diagnosing diseases, detecting illnesses, and promoting sustainable consumption [4, 5]. In addition, AA must be quantified in samples of food, pharmaceuticals, and cosmetics [6]. AA can be quantified in a number of ways to ensure human well-being and industrial productivity, such as solid phase iodine, [7], spectrophotometry [8], titrimetric [9], electrophoresis [10], fluorescence [11], chemiluminescence [12], and electrochemical techniques [13]. High-performance liquid chromatography (HPLC) allows the selective detection of a multitude of biomolecules in a mixture, but it is much slower, more expensive, and labor-intensive than traditional methods [14]. These analytical techniques are often quite expensive, labor-intensive, and difficult to use. However, electrochemical techniques have proven to be straightforward, affordable, extremely sensitive, and selective in recent years, thus attracting a great deal of attention [15]. Quantification of AA has been accomplished using two electrochemical techniques, including enzyme-based and enzyme-free techniques [16]. AA detection using enzyme-based methods is expensive and has several problems, including denaturation of enzymes during storage, so non-enzymatic methods have been extensively utilized as an alternative [17]. For non-real-time applications with higher sensitivity and selectivity than electrochemical methods, high electrocatalytic materials have always been desired [18]. It is therefore challenging to develop electrocatalytic materials with such high efficiency, but

adopting a green chemistry approach can help overcome this problem. As a result, many electrocatalytic materials have been developed and investigated for non-enzymatic sensors [19]. The strong electrochemical activity of metal oxides makes them suitable for this application [20]. Bimetallic oxides, particularly nickel–cobalt oxides (NiCo_2O_4), have been found to be excellent materials for the development of non-enzymatic sensors, owing to their significant redox properties. Since NiCo_2O_4 nanostructures have limited surface characteristics and poor electrochemical performance, they have been combined with other materials to develop composites such as $\text{MnO}_2/\text{NiCo}_2\text{O}_4$ [21], $\text{Co}_3\text{O}_4/\text{NiCo}_2\text{O}_4$ [22], NiCo_2O_4 @graphene [23] and Fe_2O_3 @ NiCo_2O_4 [24]. Moreover, numerous morphologies of NiCo_2O_4 have been fabricated including nanosphere [24], nanorods [21], nanosheets [25] and nanotubes [26]. In order to design non-enzymatic AA acid sensors with high sensitivity, new methods must be explored for improving NiCo_2O_4 electrochemical performance. The environmental friendliness, low cost, and eco-friendliness of green chemistry have drawn much attention in recent years, and it is expected to grow rapidly [23]. In a green method of mediation, biomass waste materials can be used to tailor nanostructured materials' surface properties, including catalytic sites and charge transfer properties [27]. Currently, only a few studies have been conducted on the production of NiCo_2O_4 nanostructured materials from biomass wastes. Based on the above facts, an outstanding phytochemical analysis of garlic (*Allium sativum*) leaves extract has been reported for the first time in order to modify the shape and surface properties of NiCo_2O_4 , with AA being detected highly sensitively and selectively. Among the phytochemical compounds found in garlic (*Allium sativum*) leaves extract are allicin, alliin, diallyl sulphide, S-allyl-1-cysteine, diallyl disulfide, diallyl trisulfide, allyl mercaptan, and (R)-S-(2-hydroxypropyl) cysteine [28]. Phytochemicals found in garlic leaves (*Allium sativum*) extract can create surface vacancies and modify

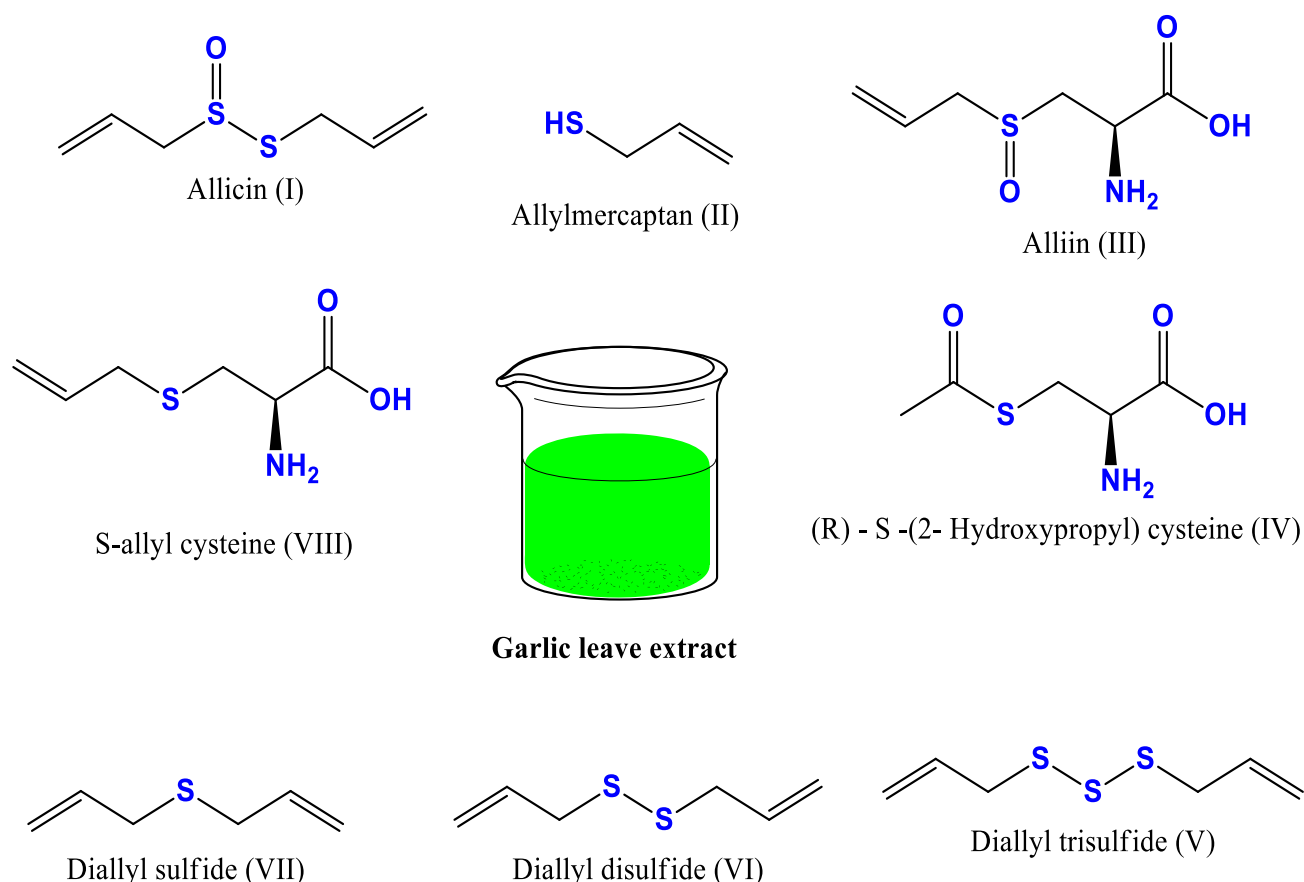
surface reactions in nanostructured materials. An illustration of phytochemicals serving as reducing, capping, and stabilizing agents can be seen in Scheme 1. In this study, garlic leaf extract served as a catalyst during the hydrothermal process to produce NiCo_2O_4 nanostructures for robotic AA determinations.

2 Experimental section

2.1 Chemical reagents used

The present study used nickel chloride hexahydrates, cobalt chloride hexahydrates ($\text{CoCl}_2 \cdot 6\text{H}_2\text{O}$), lactic acid, glucose, sodium chloride, uric acid, potassium chloride, ascorbic acid, glucose, sodium hydroxide, urea, hydrochloric acid, disodium phosphate, and monopotassium phosphate without pretreatment. Analytical grade chemical reagents were purchased from Sigma Aldrich, Karachi, and Sindh, Pakistan. A pH 7.4 phosphate buffer solution was used as the

electrolyte medium during the electrochemical determination of AA. A hydrothermal process was utilized to synthesize NiCo_2O_4 nanostructures in presence of phytochemicals. Garlic leaves were purchased at the local market, cleaned with deionized water, and allowed to air dry for five hours. The garlic leaves are then chopped and put in a juicer to make the extract. Several concentrations of garlic leaf extract, cobalt chloride hexahydrate (0.1 M), urea (0.1 M) and nickel chloride hexahydrate (0.015 M) were added to 100 mL of deionized water to produce NiCo_2O_4 nanostructures. The growth solution was diluted with different quantities of garlic leaf extract (5 mL, 10 mL, and 15 mL) to achieve a pH between 8.2 and 7.4. Total volume of precursors solution with and without the use of garlic leaves extract was equal to 100 mL. A five-hour hydrothermal reaction was then conducted with 100 mL growth solutions covered with aluminum sheets at 95 °C. Nickel–cobalt bimetallic hydroxide phase material was recovered on filter paper and repeatedly rinsed with deionized



Scheme 1 Shows the various phytochemicals present in the garlic (*Allium sativum*) extract

water. The hydroxide phase was dried for 12 h at room temperature after being collected. The bimetallic hydroxide phase of material was burned at 500 °C for five hours in the open air for the transformation of bimetallic oxide phase. Pure NiCo₂O₄ nanostructures were also synthesized without garlic leaf extract using the same method. A black colored NiCo₂O₄ nanostructured structure has been obtained, which can be utilized for further analysis.

2.2 Physical investigations of different NiCo₂O₄ nanostructures

The morphology of NiCo₂O₄ nanostructures was investigated with an SEM (JEOL Japan Model No. JSM-IT 100, Auto Fine Coater: JEC-3000FC, Coating done on a 20 mA current for 60 s), using an accelerating voltage of 10 kV. The crystal quality of garlic leaves extract NiCo₂O₄ nanostructures was determined by powder X-ray diffraction (XRD) at 45 kV and 45 mA utilizing CuK radiation ($\lambda = 1.5418 \text{ \AA}$) as a source of X-rays. To examine the confined nanoscale structure, a 200 kV high resolution transmission electron microscope (HRTEM) was used. An energy dispersive spectrometer was used to quantify the elemental mapping. The valence states of the molecules were confirmed by X-ray photoelectron spectroscopy (XPS) under extremely high vacuum. The XPS features were deconvolved using a Shirley type background and Voigt curves with C1s at 284.6 eV as the reference binding energy.

2.3 Non-enzymatic sensing of AA onto surface modified NiCo₂O₄ nanostructures

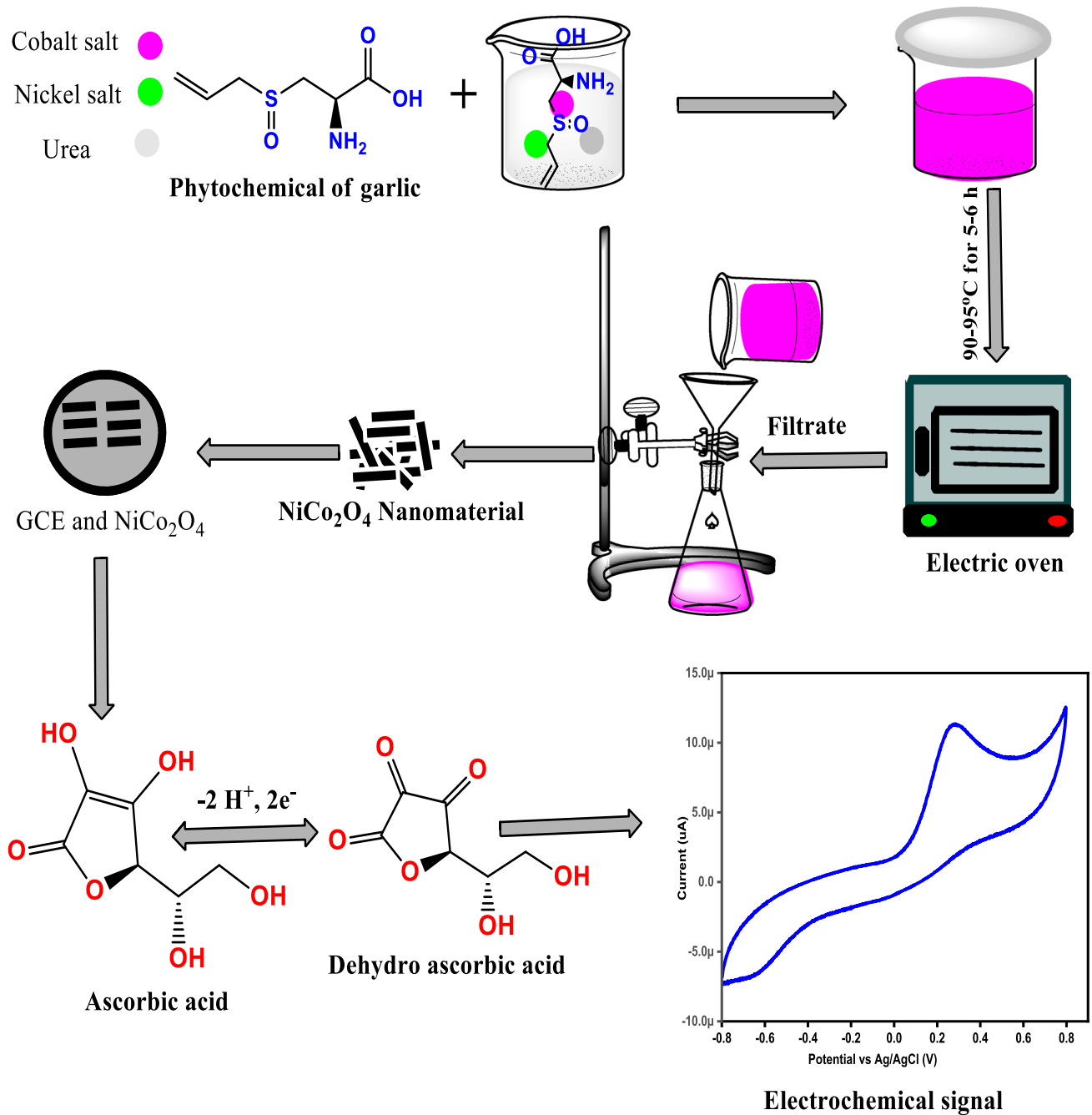
A variety of electrochemical techniques have been used to characterize non-enzymatic AA sensors, including cyclic voltammetry, amperometry, electrochemical impedance spectroscopy, and linear sweeping voltammetry. This experiment was conducted with a three-electrode configuration, consisting of silver-silver chloride (Ag/AgCl, filled with 3.0 M KCl) serving as the reference electrode, platinum sheet serving as the counter electrode, and glassy carbon electrode (GCE) serving as the working electrode. The GCE was washed with deionized water before modification and polished with alumina paste (0.3 μm) and silicon paper. An ink containing ten mg of NiCo₂O₄ nanostructures and 0.5 mL of

Nafion (5%) was prepared with 2.5 mL of deionized water and 0.5 mL of Nafion. A 10 μL of catalyst ink (mass of 0.2 mg) was dropped onto the GCE using drop casting method and dried with the blow of air at room temperature. An AA stock solution of 10 mM was prepared in a buffer solution of 0.1 M phosphate buffer at pH 7.4. In this solution, AA was dissolved in phosphate buffer. The selectivity of non-enzymatic AA sensors was tested by diluting AA solutions in buffer solutions containing potassium, sodium, and potassium ions at pH 7.4. The sensor was tested using interfering species at the same concentration of AA, including urea, lactic acid, glucose, and uric acid. The linear range of the AA sensor was determined using CV and chronoamperometry methods using different concentrations of AA dissolved in 0.1 M phosphate buffer solution (PBS), pH 7.4. The technique allowed a non-enzymatic sensor's low limit of detection to be determined [29]. A schematic representation of the synthesis, electrochemical signal, and the general mechanism for sensing ascorbic acid is shown in Scheme 2. Furthermore, the electrochemical cell set up is shown in Scheme 3.

3 Results and discussion

3.1 Structural and morphological investigations of garlic leaves extract assisted different NiCo₂O₄ nanostructures

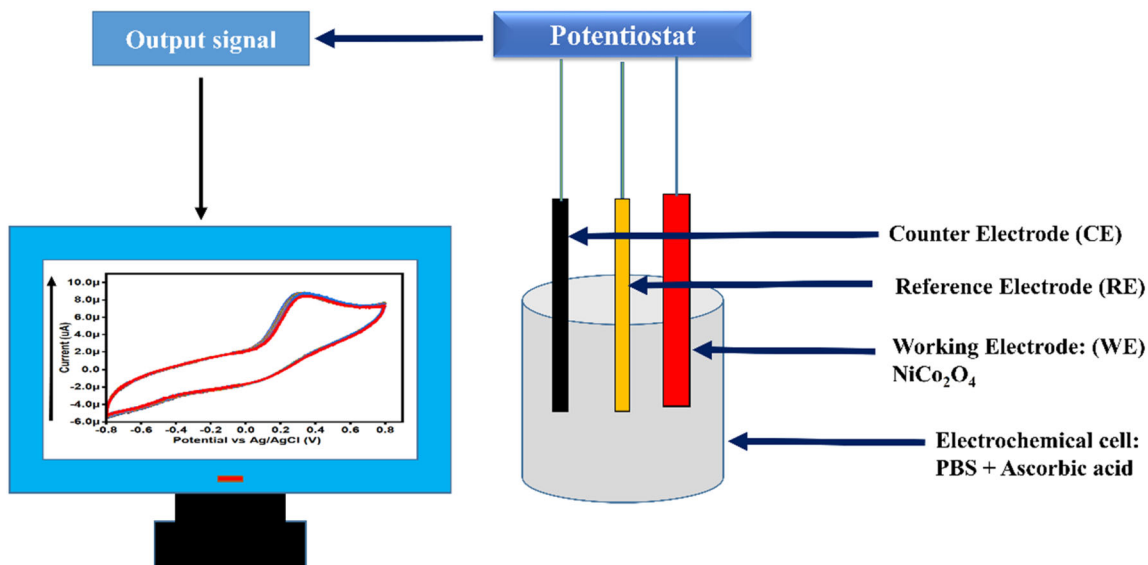
A powder XRD pattern of NiCo₂O₄ nanostructures is illustrated in Fig. 1, which can be used to evaluate the crystallinity of the powder. Phytochemical components in garlic leaf extract have also been shown to improve NiCo₂O₄ nanostructure crystal quality. The measured diffraction patterns matched the standard JCPDS card no: 96-900-5891 closely, attesting a cubic crystal phase of the material and confirming its high purity. Typical NiCo₂O₄ nanostructure reflections are (111), (220), (311), (222), (400), (511) and (440), at two theta angles of 19.40, 31.30, 36.880, 38.590, 44.850, 59.410, and 65.300. In spite of the fact that garlic leaf extract did not alter the crystal cubic phase or composition of NiCo₂O₄ nanostructures, the relative intensities were slightly varied due to the reducing, capping, and stabilizing properties of garlic leaf extract, as shown in Fig. 1. NiCo₂O₄ nanostructures were examined using SEM in Fig. 2a–e. Figure 2a



Scheme 2 Stepwise synthesis of NiCo₂O₄ nanostructures using garlic leaves extract and general oxidation mechanisms of AA using electroanalytical method

illustrates a pure NiCo₂O₄ nanostructure with a nanorod-like morphology and several microns in length. In Fig. 2b–e, garlic leaf extract altered the morphology of NiCo₂O₄ nanostructures, resulting in short-range thinner nanowires consisting of nanoparticles rather than nanorods, demonstrating the impact of phytochemicals on surface morphology. According to Fig. 2e, NiCo₂O₄ nanostructures

obtained with garlic leaf extract are typically 50–100 nm in size, confirming the capping, reducing, and stabilizing roles of garlic leaf extract. By incorporating phytochemicals into garlic leaf extracts, NiCo₂O₄ nanostructures may be structurally modified. Nanorods were transformed into thinner nanowires due to oxygenated groups terminated from garlic leaf extract, as shown in Scheme 1. In the



Scheme 3 illustrates the electrochemical cell set up

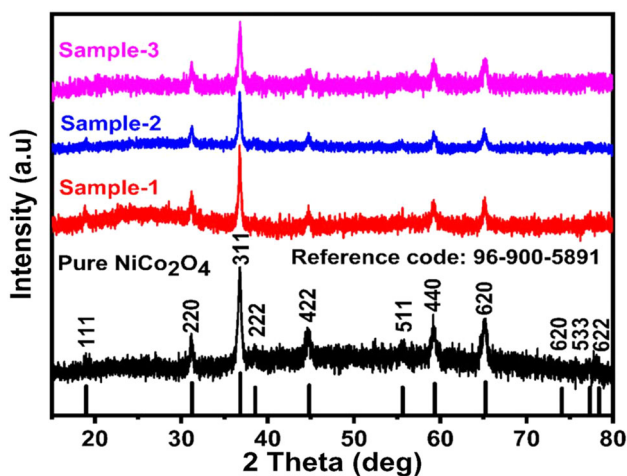


Fig. 1 XRD Patterns of various NiCo_2O_4 nanostructures including pristine and prepared with 5 mL (Sample 1), 10 mL (Sample 2) and 15 mL (Sample 3) of garlic leaves extract

process of growing, phytochemicals played a vital role in transforming nanorods into thinner nanowires due to their reducing, capping, and stabilizing properties. Using Image J software, HRTEM and fast Fourier transform (FFT) images were taken to examine deep morphological features and atom-by-atom calculate d-spacing of NiCo_2O_4 nanostructures. In Figs. 3 and 4, HRTEM analysis is shown on pristine NiCo_2O_4 nanostructures and garlic leaf extracts of 10 mL assisted synthesized NiCo_2O_4 nanostructures. Figure 3 shows the first TEM/HRTEM analysis, the elemental mapping, and the EDS spectrum for pure

NiCo_2O_4 nanostructures. According to Fig. 3a, the calculated d-spacing for pristine materials is 0.46 nm as calculated using Image-J software [30, 31]. The EDS spectra and elemental maps of pristine material are shown in Fig. 3b–e. The NiCo_2O_4 nanostructures prepared with garlic leaves extract have also shown a reduction in d-spacing compared with pure NiCo_2O_4 , as shown in Fig. 4a, along with the desired FFT transformation [32, 33]. Figure 4b–e illustrates the elemental mapping with corresponding EDS spectra. Garlic leaf phytochemicals have demonstrated their ability to reduce, color, and stabilize materials due to their reduced d-spacing values. Using a synthetic garlic leaf extract, researchers have observed more active sites, vacancies, and electrochemical activity towards facilitating electron transfer between electrodes [34]. The possible synthesis mechanism of NiCo_2O_4 using phytochemicals from the garlic leaves extract as described in Scheme 4. Briefly, it could be illustrated that the functional groups like amine and hydroxyl from phytochemicals of garlic leaves extract could show the chelating possibilities with the bimetallic ions along with hydroxyl ions produced by the reaction of urea with the water through the ammonia formation. Hence, significant morphological transformation of NiCo_2O_4 might take place as shown in Scheme 4.

Furthermore, XPS measurements were conducted as shown in Fig. 5 in order to gain a better understanding of the chemical states and surface species of NiCo_2O_4 nanostructures prepared with garlic leaf

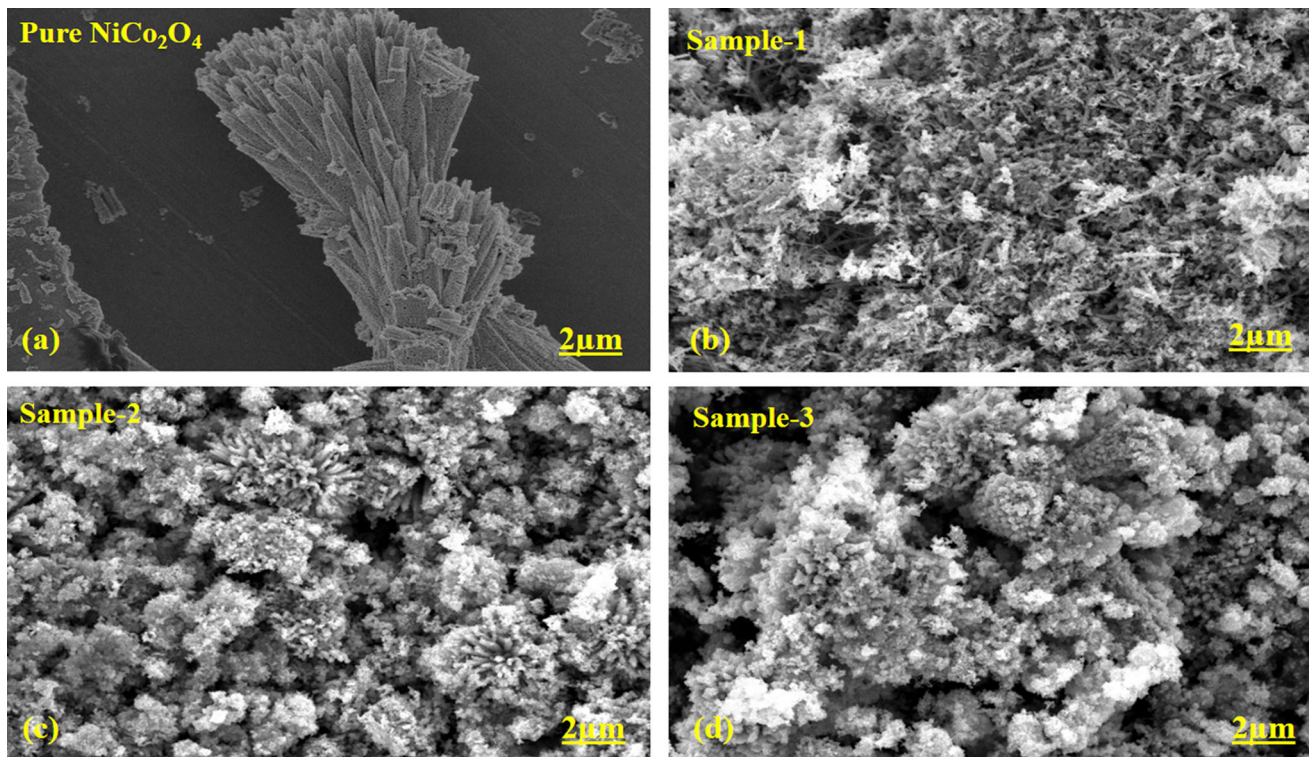


Fig. 2 a–d SEM images of various NiCo₂O₄ nanostructures including pristine and prepared with 5 mL (Sample 1), 10 mL (Sample 2) and 15 mL (Sample 3) of gallic leaves extract

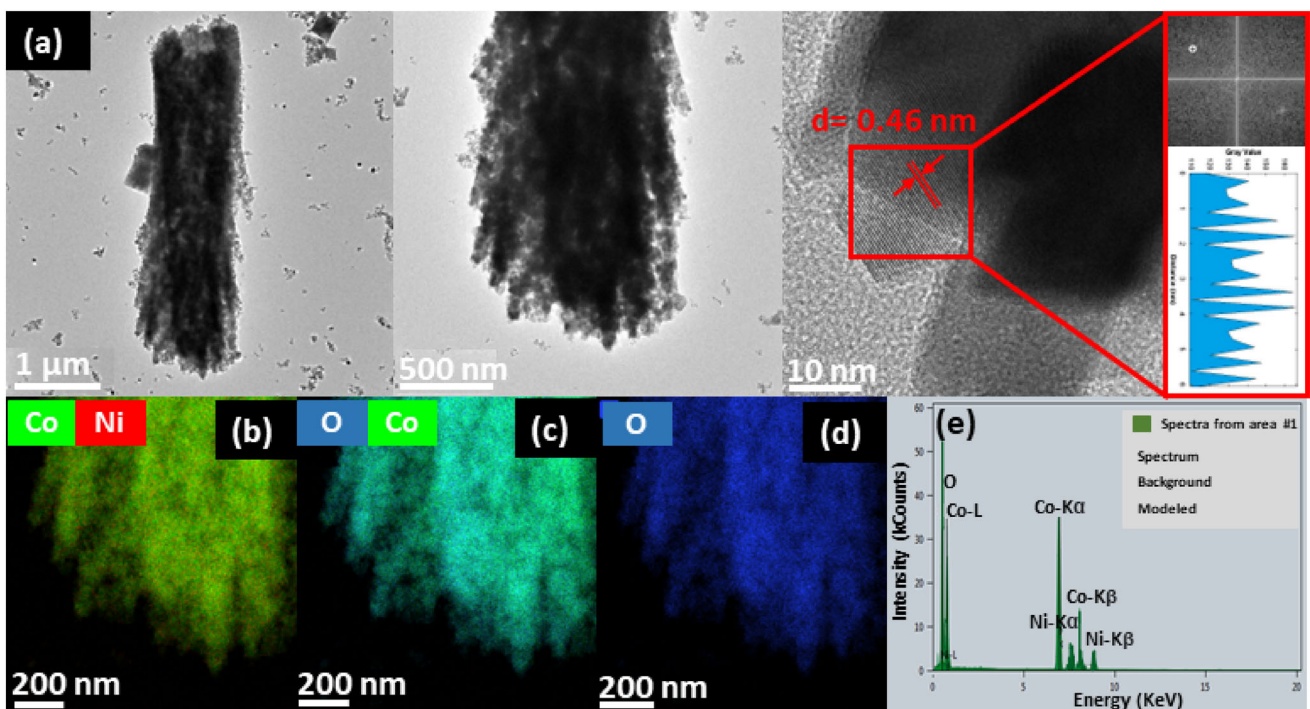


Fig. 3 HRTEM analysis of pristine NiCo₂O₄ nanostructures a HRTEM images and FFT conversion at right side with d-spacing value, b–d corresponding elemental mapping, e EDS spectra for elemental existence

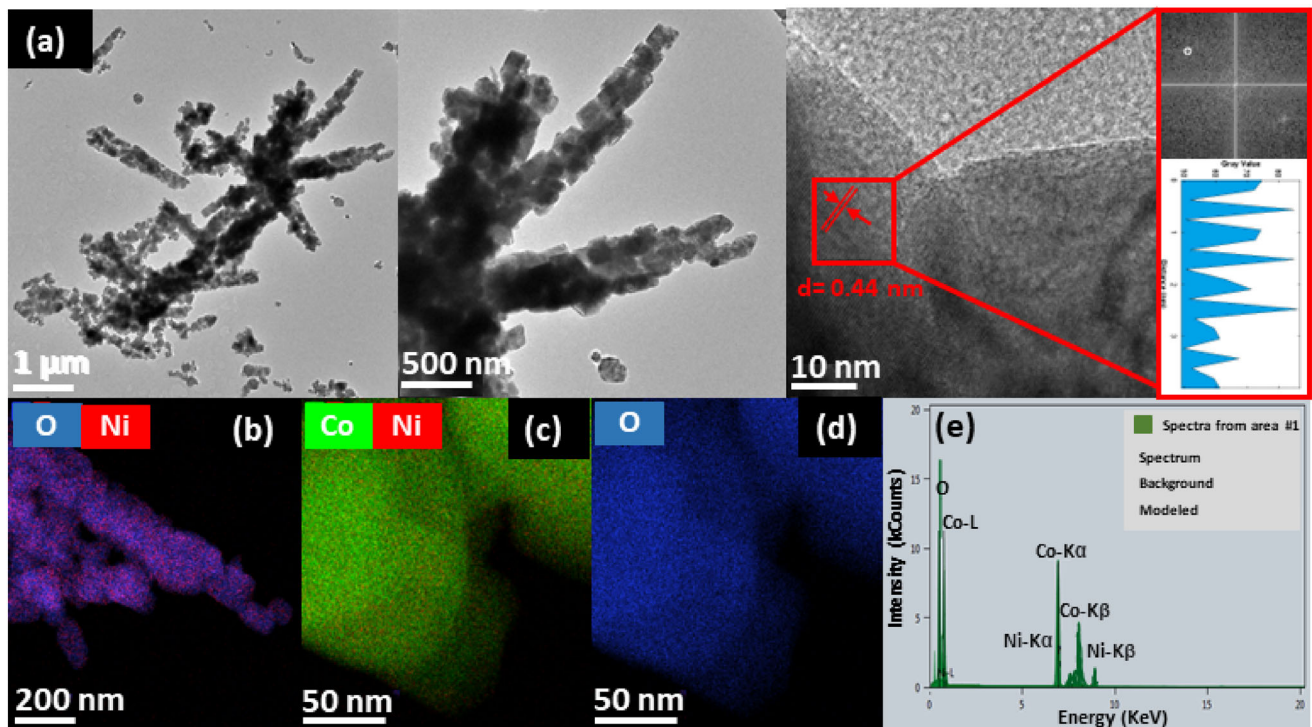


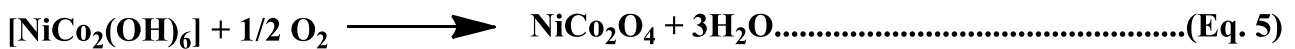
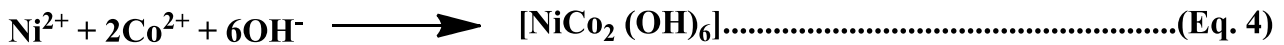
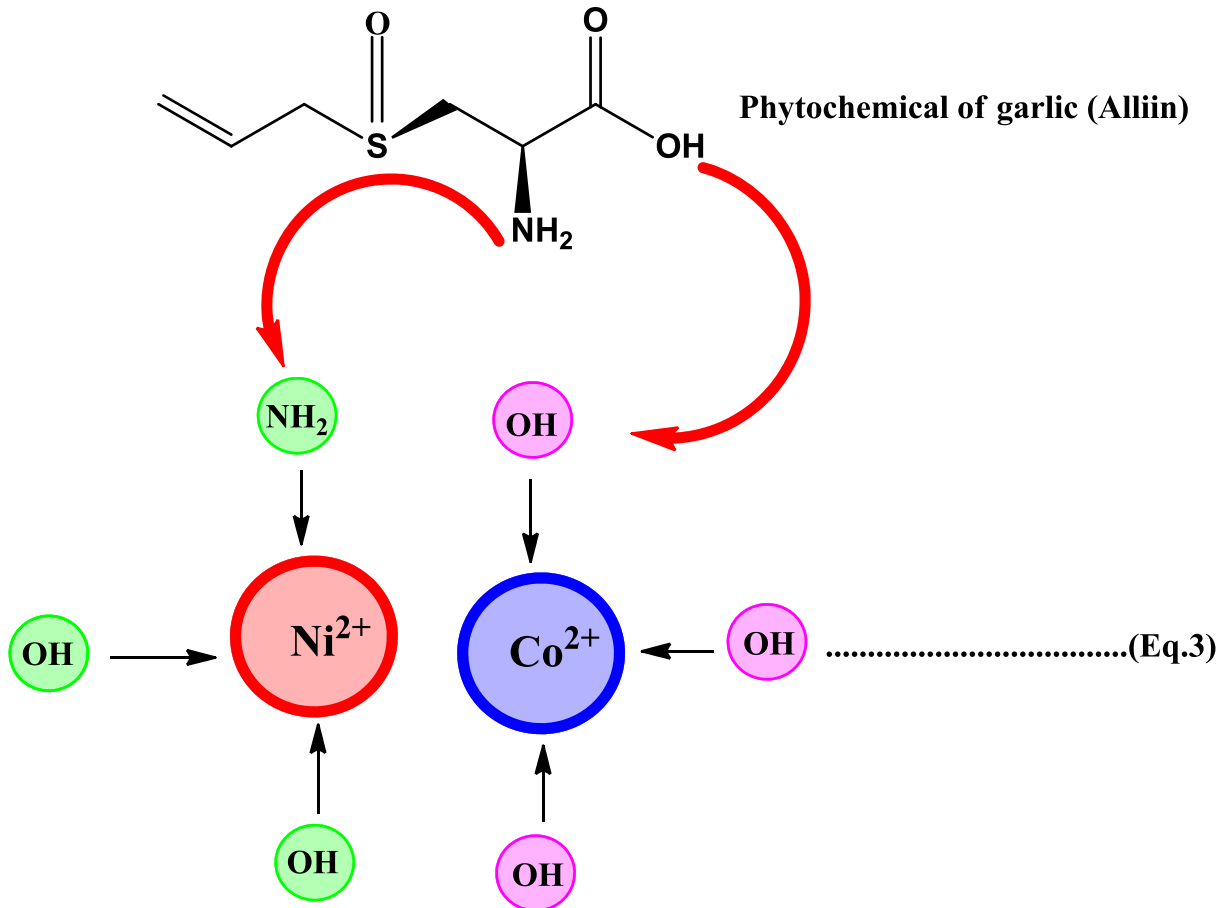
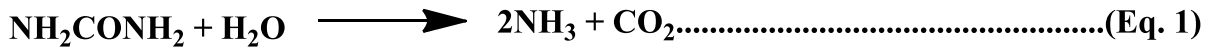
Fig. 4 HRTEM analysis of NiCo_2O_4 nanostructures prepared with 10 mL of garlic leaves extract **a** HRTEM images and FFT conversion at right side with d-spacing value **b–d** corresponding elemental mapping, **e** EDS spectra for elemental existence

extract. Since pristine NiCo_2O_4 nanostructures have been reported previously [70], both with and without garlic leaves extract, the method used here is similar. Carbon's average binding energy was determined based on the XPS binding energies of each element. NiCo_2O_4 nanostructures contain two different chemical states of Co, as shown in Fig. 5a. Figure 5a shows two spin orbital peaks located at 779.73 eV and 781.60 eV, corresponding to Co^{3+} and Co^{2+} oxidation states, respectively. Additionally, satellite peaks at 785.8 eV and 789.37 eV were observed in the resolved Co 2p spectrum. Co^{3+} and Co^{2+} were calculated to have a relative percentage of 60.18% and 27.29%, respectively. The Ni 2p spectrum is shown in Fig. 5b using the Voigt fitting. As shown in Fig. 5b, Ni^{2+} and Ni^{3+} valence states exhibit a spin orbital double peak at 853.88 eV and 855.60 eV, respectively. In terms of valence percentage, Ni^{2+} represents 6.06% and Ni^{3+} represents 67.38%. An 861.34 eV satellite peak was observed with a relative percentage of 25.96%. XPS fits for Ni 2p have been shown to be in agreement with previous results [21, 35]. The O 1s spectrum of NiCo_2O_4 nanostructures prepared with 10 mL of garlic leaf extract was also collected, and its fitting results are shown in Fig. 5c. The

binding energies estimated at 529.69 eV, 531.10 eV, and 532.68 eV for well resolved three peaks have been associated with distinct metal–oxygen, oxygen ions, and physic/chemisorbed water on the surface of NiCo_2O_4 nanostructures, confirming earlier result [35]. Studies have shown that NiCo_2O_4 nanostructures prepared with garlic leaf extract have high oxygen ions (O^-) and Co^{3+} valence states that are highly desirable for electrocatalysis [21].

3.2 Non-enzymatic sensing of ascorbic acid (AA) using NiCo_2O_4 nanostructures prepared with garlic leaves extract

An electrolyte of pH 7.4 phosphate buffer solution was used for the development of AA sensors. Three-electrode cells were used for the detection of AA. For each electrode, preliminary electrochemical signals were obtained using cyclic voltammetry, as shown in Fig. 6a. Four GCEs were modified with pure NiCo_2O_4 nanostructures and three samples of NiCo_2O_4 nanostructures prepared with 5 mL, 10 mL, and 15 mL of garlic leaves extract. They were represented as modified glassy carbon electrode (MGCE). As shown in Fig. 6a, CV curves were recorded using



Scheme 4 Possible synthesis mechanism of NiCo₂O₄ nanostructures using phytochemicals from garlic leaves extract

0.5 mM AA at a scan rate of 50 mV/s. Compared to pristine NiCo₂O₄ nanostructures, NiCo₂O₄ nanostructures prepared with garlic leaves extract show strong oxidation signals in Fig. 6a. A 5 mL concentration of garlic leaf extract enhanced NiCo₂O₄ nanostructure electrochemical performance, while a 10 mL concentration of garlic leaf extract resulted in the best electrochemical performance. By adding garlic leaves extract to NiCo₂O₄ nanostructures, the

effectiveness of these structures significantly decreased, possibly due to a decrease in active sites. NiCo₂O₄ nanostructures' functionality was limited by a 15 mL use of garlic leaves extract since the surface became less active and had favorable features that could facilitate AA oxidation. According to Fig. 6b, NiCo₂O₄ nanostructures and bare glassy carbon electrodes (BGCE) were tested in phosphate buffer solutions at pH 7.4 in the presence and absence of

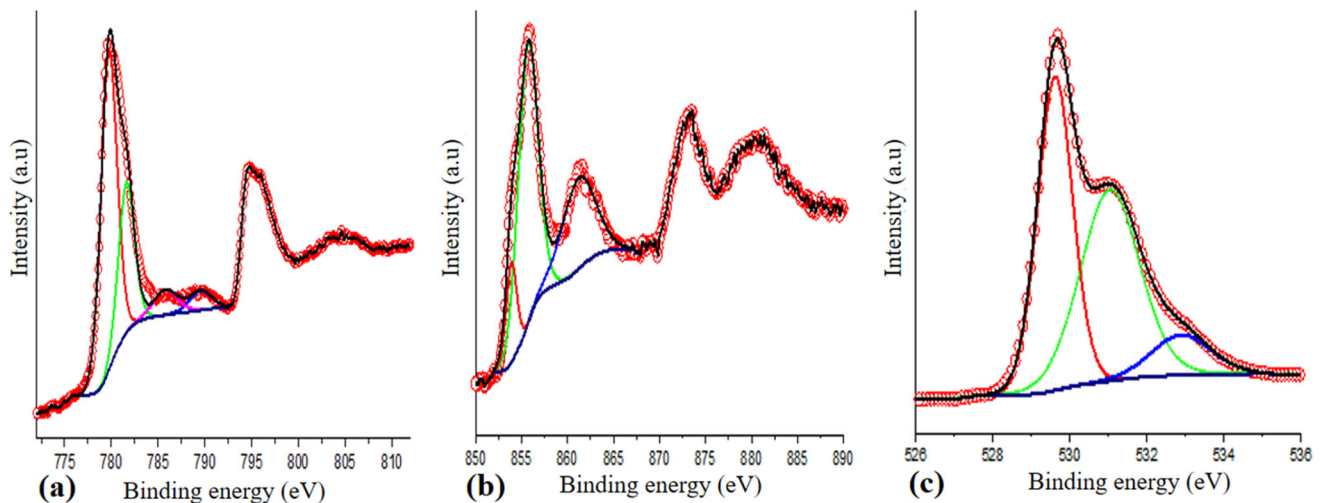


Fig. 5 XPS resolved spectra **a** Co $2p$, **b** Ni $2p$, **c** O $1s$ of NiCo_2O_4 nanostructures prepared with 10 mL of galric leaves extract

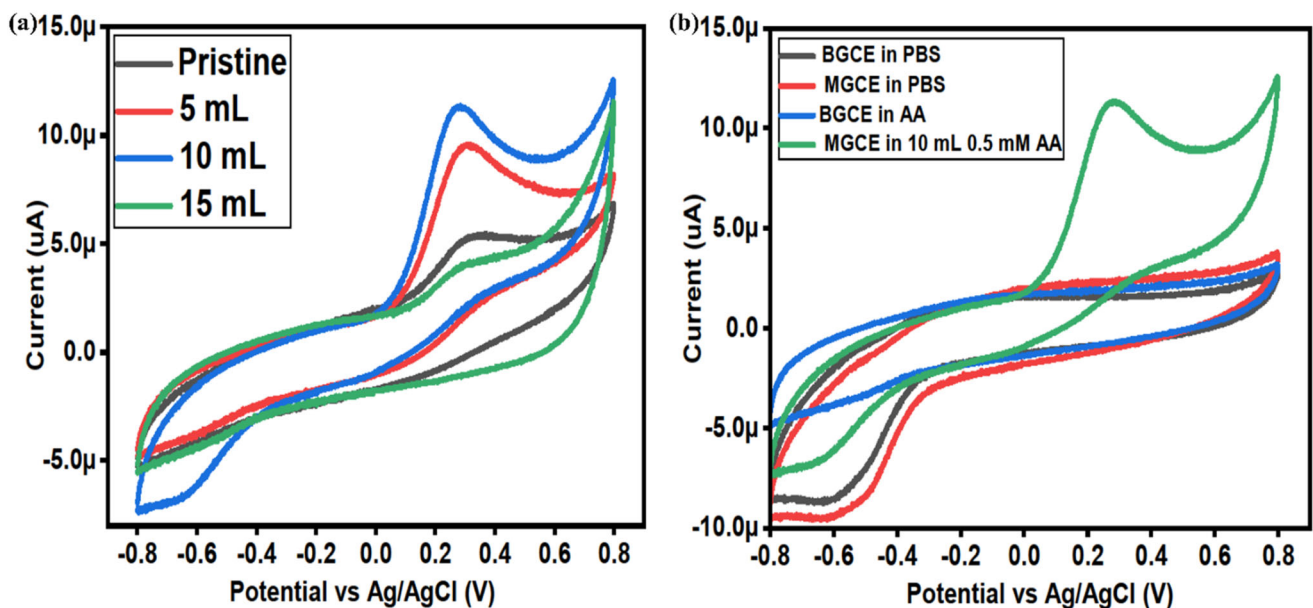


Fig. 6 a Cyclic voltammograms at a scan rate of 50 mV/s of MGCE with 5 mL, 10 mL and 15 mL galric leaves extract assisted NiCo_2O_4 and pristine NiCo_2O_4 -modified GCE in the presence of 0.5 mM of AA in 0.1 M PBS pH 7.4. **b** Cyclic voltammograms at

50 mV/s of bare GCE and modified with 10 mL assisted NiCo_2O_4 in electrolyte and in the presence of 0.5 mM AA in 0.1 M PBS pH 7.4

0.5 mM AA. As shown in Fig. 6b, NiCo_2O_4 nanostructures generated the AA signal, whereas bare glassy carbon electrodes did not demonstrate any electrochemical activity. In response to this preliminary testing, systematic sensor studies were conducted with NiCo_2O_4 nanostructures prepared using galric leaf extract in 10 mL. In an experimental study using NiCo_2O_4 nanostructures, the following mechanism was demonstrated to detect AA. Typical electron transfer reactions involve oxidizing AA to give

electrons to Co^{3+} and Ni^{3+} ions, then reducing them to Co^{2+} and Ni^{2+} . NiCo_2O_4 nanostructures synthesized with 10 mL of galric leaf extract showed enhanced oxidation because they were exposed to a high density of active sites, had favorable charge transfer at electrode-electrode interfaces, and had unique morphological characteristics resulting from reducing, capping, and stabilizing agents from galric leaves extract. Figure 7a shows the electrochemical kinetics of nanostructures prepared with 10 mL of

garlic leaf extract and 0.5 mM AA at different scan rates. The diffusion-controlled kinetics of AA electrochemical reaction were demonstrated by increasing the scan rate and increasing the peak current. Figure 7b illustrates the peak currents of oxidation for each scan rate against the square root of the scan rate, and literature supports these findings [35–38]. There was a regression coefficient of 0.99 during the scan rate study in the presence of AA oxidation, which was regulated by surface adsorption and electrochemistry [38, 39]. AA oxidation was investigated using CV curves at different pH values adjusted in 0.5 mM of AA, and the results are shown in Fig. 8a. An AA sensor that is nonenzymatic was evaluated at pH 7.4 since the peak shape and current are more obvious. In the pH investigation, the pH of the analyte solution significantly influenced NiCo₂O₄ nanostructure activity, as has already been reported [39]. The pH of the solution influences the limited activity of NiCo₂O₄ nanostructures, as shown in Fig. 8b. This indicates that analytes with a pH close to 7.4 exhibit favorable oxidation of AA, but analytes with a pH below or above 7.4 are less stable and effective. Previous studies have documented such phenomena [40]. As a result of analyzing the pH ranges of 5.4, 6.4, 7.4, 8.4 and 9.4, it is determined that all electrochemical experiments were conducted at

pH 7.4, as the CV results shown are highly stable at pH 7.4 and show an enhanced oxidation peak.

3.3 The calibration plots, stability, repeatability and selectivity studies of newly developed non-enzymatic AA sensor based on surface modified NiCo₂O₄ nanostructures

With 10 mL of garlic leaf extract, NiCo₂O₄ nanostructures were prepared to study the linear range and limit of detection of AA. The sensing range of NiCo₂O₄ nanostructures prepared with 10 mL of garlic leaves extract was maintained using different electrochemical modes. However, different linear AA ranges were observed depending on the sensitivity of each electrochemical mode. We determined the linear range of AA concentrations in phosphate buffer solution at pH 7.4 using CV at 50 mV/s using a range of AA concentrations in phosphate buffer solution. Figure 9a shows that the peak current for AA oxidation increased linearly with increasing AA concentrations, with a linear range of AA of 0.5 to 8.5 mM. From the results of this study, it appears that AA non-enzymatic sensors have a wide linear range among those reported so far [41–46]. The linear plot depicted in Fig. 9b was constructed to evaluate the analytical quality of a newly constructed non-

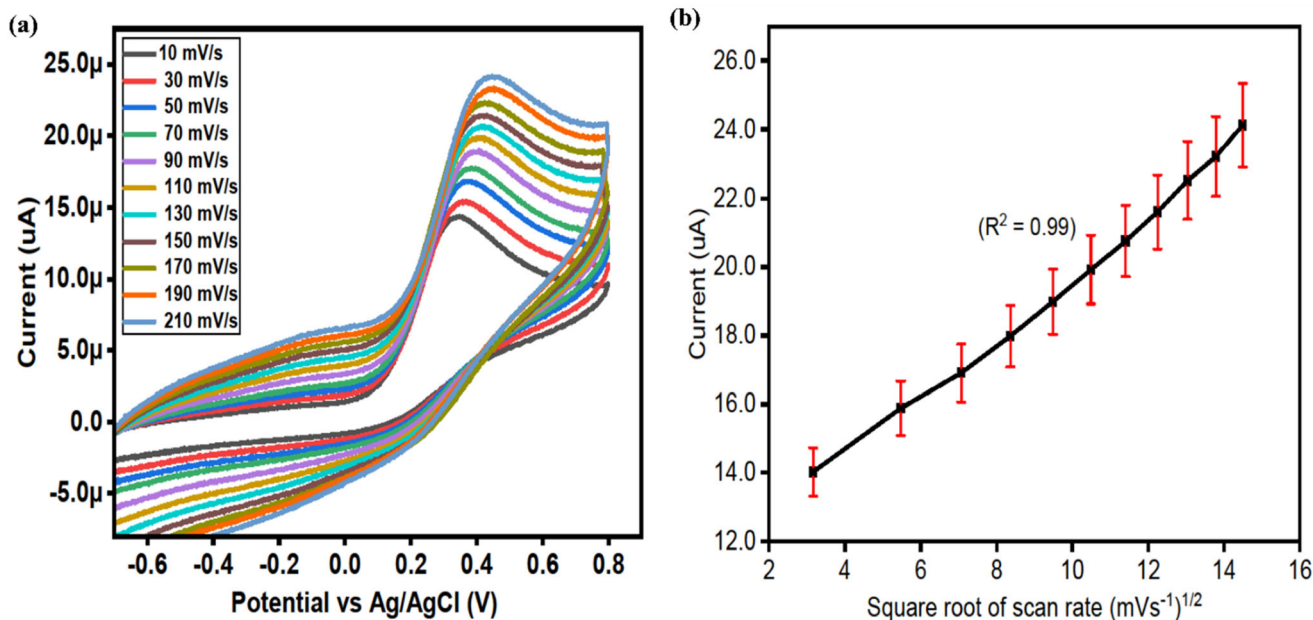


Fig. 7 a Cyclic voltammograms at a scan rate of 50 mV/s of MGCE with 10 mL garlic leaves extract assisted NiCo₂O₄ modified GCE in the presence of 0.5 mM of AA in 0.1 M PBS pH 7.4. b Linear plot of peak current against square root of scan rate

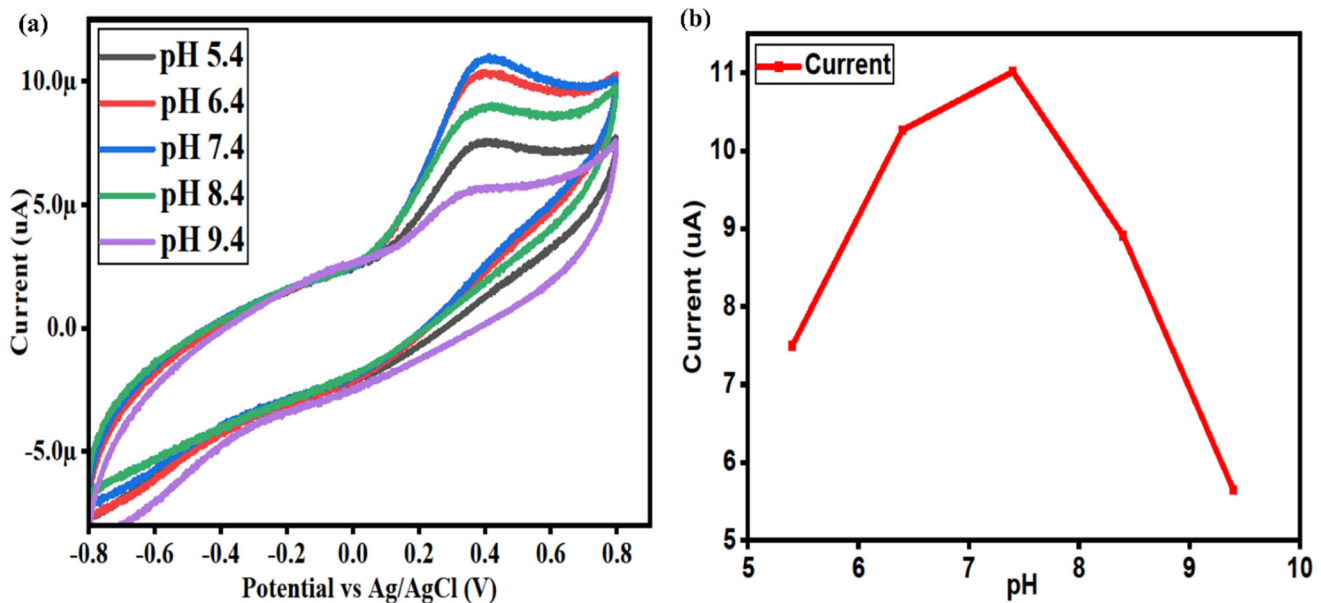


Fig. 8 a Cyclic voltammograms at a scan rate of 50 mV/s of MGCE with 10 mL of garlic leaf extract assisted NiCo_2O_4 -modified GCE in the presence of different pH values of 0.5 mM of

AA in 0.1 M PBS. **b** Linear plot of peak current versus different pH values of 0.5 mM of AA in 0.1 M PBS

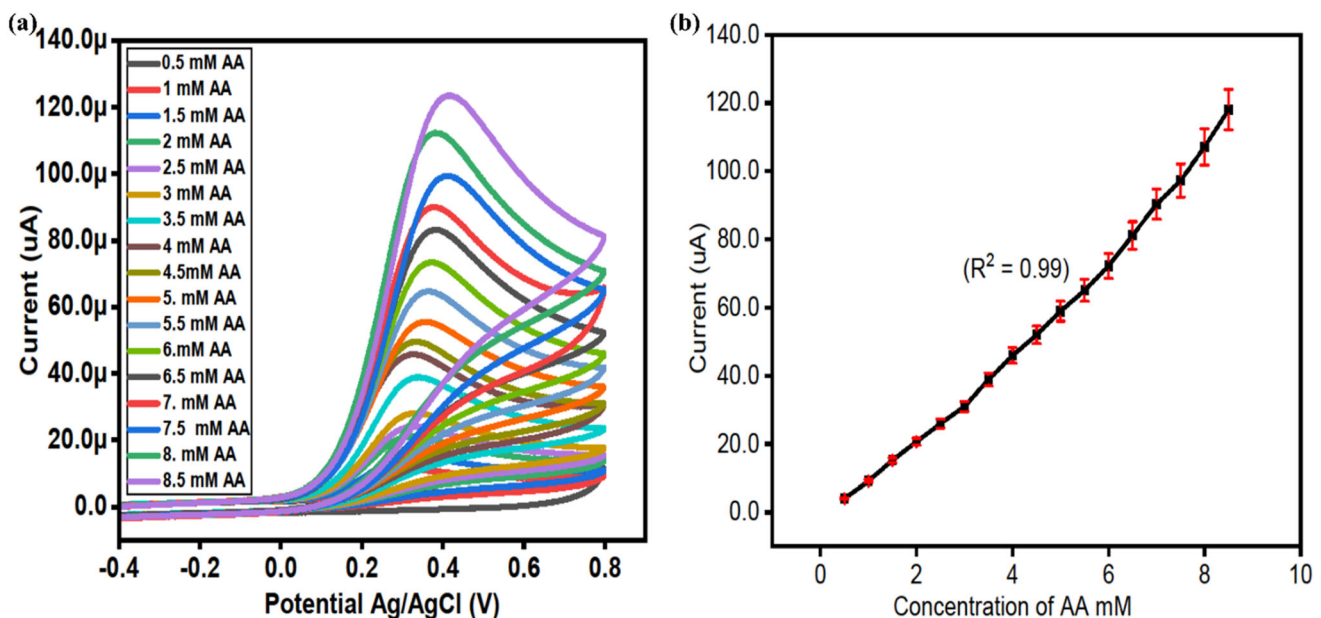


Fig. 9 a Cyclic voltammograms at a scan rate of 50 mV/s of MGCE with 10 mL of garlic leaves extract assisted NiCo_2O_4 in the presence of various concentrations of AA in 0.1 M PBS pH 7.4. **b** Linear plot of peak current versus successive increase of AA concentrations

enzymatic AA sensor in terms of accuracy and precision by selecting the oxidation peak current for each AA concentration against a variety of AA concentrations. According to the linear plot of CV data, AA sensors are capable of measuring high concentrations of AA and can be applied to the analysis of real samples. The limits of detection (LOD) and

quantification (LOQ) were estimated using published research [41]. This study determined that the LOD and LOQ were 0.01 mM and 0.04 mM, respectively. The reported results shown in Table 1 based on the non-enzymatic AA, it is very clear that the suggested approach to AA analysis could prove highly valuable as a substitute technique for AA detection in real

Table 1 Performance comparison of the enzyme-free sensor based on NiCo₂O₄ nanostructures grown with 10 mL garlic leaves extract versus several non-enzymatic AA sensors in the literature

Sensing electrode material	Linear range (μM)	Detection of limit (μM)	References
NPG	10–1100	2.0	[48]
GCE/Au@Pd-RGO	0.01–100	0.002	[49]
PdAu/rGO/GCE	12.5–700	12.5	[50]
Au-IDA/hCNT	0–600	20	[51]
Graphene-AuNPA/SPA	20–375	1.04	[52]
AuNP/PPy/TiO ₂	1–5000	0.1	[53]
S/NP-Au	0.3–923.3	0.0263	[54]
CuNPs/PANI/GCE	3–3500	2	[55]
ZnO-Cu _x /PPy/GCE	200–1000	25	[56]
PPy/hydrogel/GCE	2.5–1500	1.28	[57]
PANI-HNTs/TTO	5–5500	0.21	[58]
PANI-PMB/CPE	4–110	1.3	[59]
Pd/CNF-CPE	50–4000	15	[59]
RGO/GCE	30–350	14.8	[60]
Co ₃ O ₄ /GCE	500–6500	1	[61]
MWCNT/CCE	15–800	7.71	[62]
OMC/Nafion	40–800	20	[63]
Au/Ru nanoshells /GCE	5–2000	2.2	[64]
Chitosan-graphene	50–1200	50	[65]
NiCo ₂ O ₄ nanostructure (garlic leaves extract)	500–8500	10	Present work

samples where a broad linear range and a low detection limit are highly desirable. As well, the linear sweep voltammetry (LSV) mode was used to estimate the calibration of a newly constructed non-enzymatic AA sensor, as shown in Fig. 10a. Fig. It is shown in Fig. 10a how the proposed AA sensor arrangement can detect AA over a wide linear range, 0.1 mM to 7.0 mM, and generate measurable currents. As the concentration of AA increases, a greater current is produced, demonstrating the sensitivity of the recently designed AA sensor. A linear plot of peak current against AA concentration is shown in Fig. 10b. The proposed non-enzymatic AA sensor exhibits outstanding analytical performance and has a coefficient of 0.99 as a regression coefficient based on a linear fitting of LSV curves. Based on a full CV curve, an AA sensor can detect a wide linear range of AA with precise and accurate outputs. Figure 11a illustrates how the linear range of the AA sensor can also be calculated using the extremely sensitive electrochemical mode of amperometry. When the concentration of AA was between 0.5 and 3.5 mM, the amperometric signal was highly sensitive. Figure 11b shows a linear plot of the amperometric signal for these various AA concentrations. This

analysis shows that the powerful analytical features of AA detection are capable of detecting AA with a regression coefficient of 0.99. The excellent electrochemical activity of NiCo₂O₄ nanostructures prepared with 10 mL garlic leaf extract has been attributed to several factors, including oxygen vacancies on the surface, good crystal quality, surface modification by reducing agents, and well controlled size and shape due to the capping agent Several and stabilizing agents of garlic leaf extract phytochemicals. Analytical techniques such as SEM, XRD, HRTEM, and XPS have confirmed the results. In order to determine how well the proposed AA sensor performs in the presence of potential interfering species, a selectivity experiment was conducted. The interfering study was used to investigate the selectivity of proposed non-enzymatic sensor and the concentration of ascorbic acid was used as 0.5 mM, whereas the concentration of each interfering agents was used about 0.1 mM. In Fig. 12a, we have plotted CV curves with interfering species such as glucose, uric acid, urea, lactic acid, mannose, sodium ions, chloride ions, potassium ions, and calcium ions at 50 mV/s in 0.5 mM AA. In the presence of AA, successive additions of interfering species did not

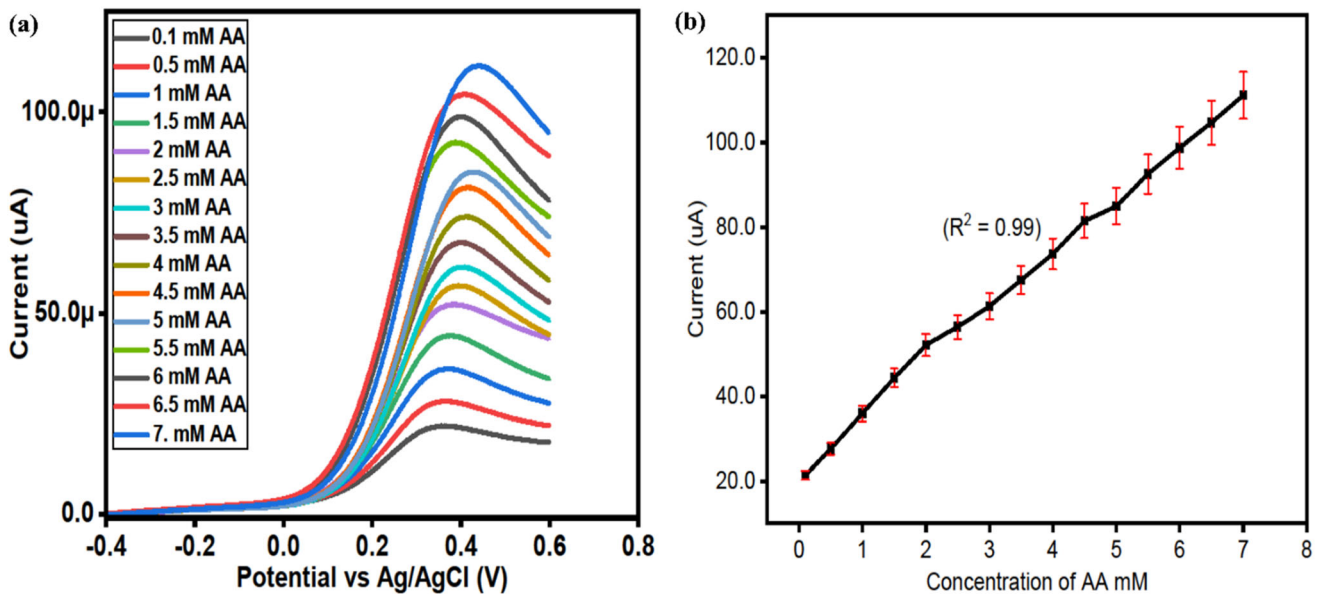


Fig. 10 a Linear sweep voltammetry at a scan rate of 10 mV/s of MGCE with 10 mL of garlic leaves extract assisted NiCo_2O_4 in the presence of various concentrations of AA in 0.1 M PBS pH 7.4.

b Linear plot of peak current versus successive increase of AA concentrations

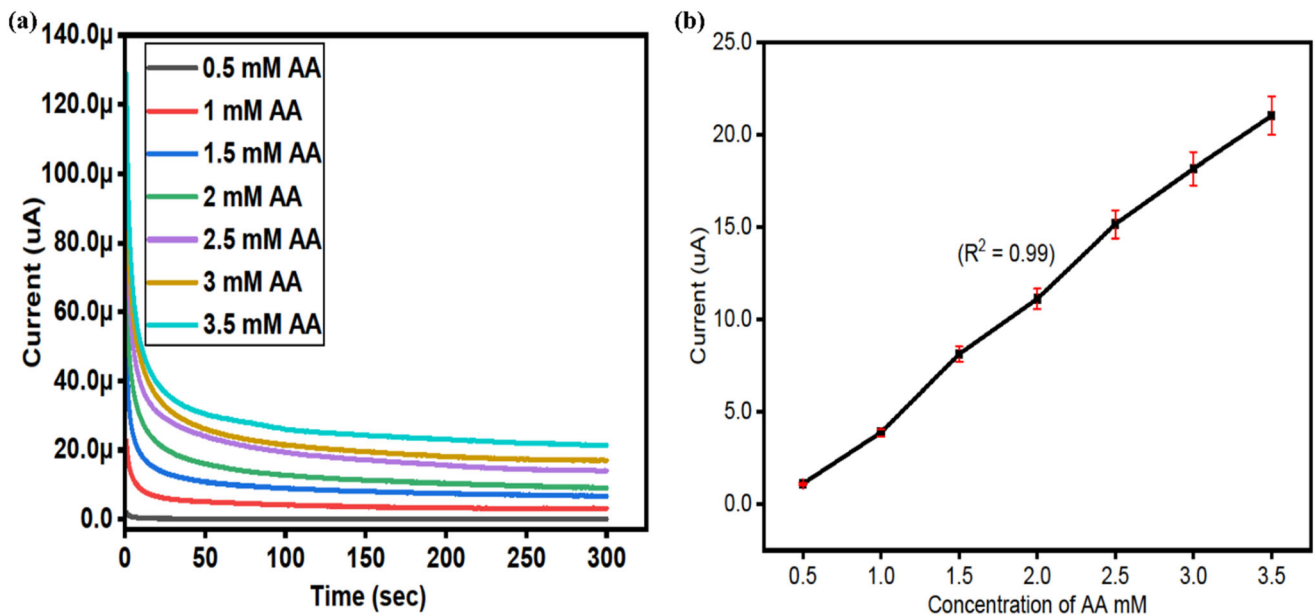


Fig. 11 a Chronoamperometric response curves measured at an applied potential of 0.3 V of MGCE with 10 mL of garlic leaves extract assisted NiCo_2O_4 in the presence of various concentrations

of AA in 0.1 M PBS pH 7.4. **b** Linear plot of peak current versus successive increase of AA concentrations

affect the oxidation peak position, drift in oxidation potential, or peak current of the AA sensor. In this study, the proposed AA sensor configuration was found to have excellent selectivity and may be suitable for detecting AA in biological matrixes. In Fig. 12b, a bar graph shows the peak current

variation of AA following the addition of interfering species. Peak current changes by less than 4%. NiCo_2O_4 nanostructures can selectively quantify AA even in the presence of competing interference agents by reducing, capping, and stabilizing the phytochemicals in garlic leaves extract. The AA sensor

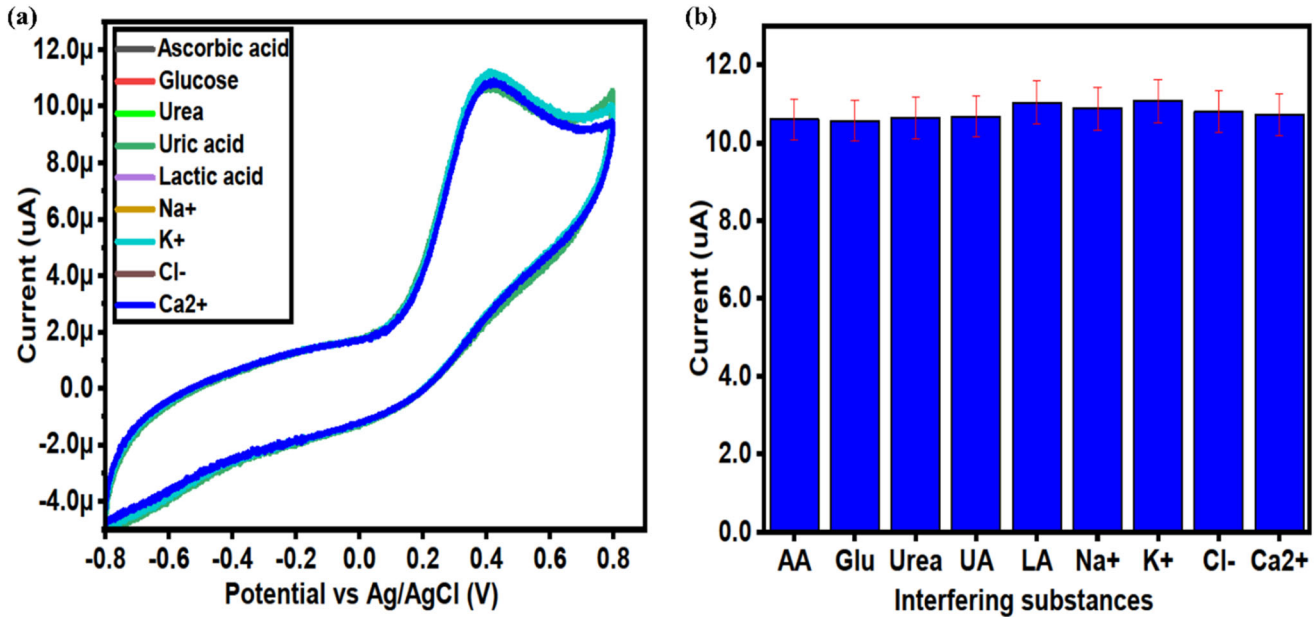


Fig. 12 a Cyclic voltammograms at a scan rate of 50 mV/s of MGCE with 10 mL of garlic leaves extract assisted NiCo₂O₄ in the presence of 0.5 mM AA and other competing interfering agents

(20%) in 0.1 M PBS pH 7.4. **b** Bar graph of peak current with addition of interfering species for the illustration of variation of peak current

electrode was evaluated for repeatability and stability by measuring 20 CV cycles of 50 mV/s at 0.5 mM. Figure 13a shows that the gadget can be repeatedly used. Enzymatic biosensors are particularly problematic when it comes to the stability of AA

biosensors. Therefore, we developed a non-enzymatic AA sensor for practical sample analysis. As shown in Fig. 13b, a bar graph shows peak current after several repeatable CV cycles. A low error rate of less than 5% demonstrates that the presented

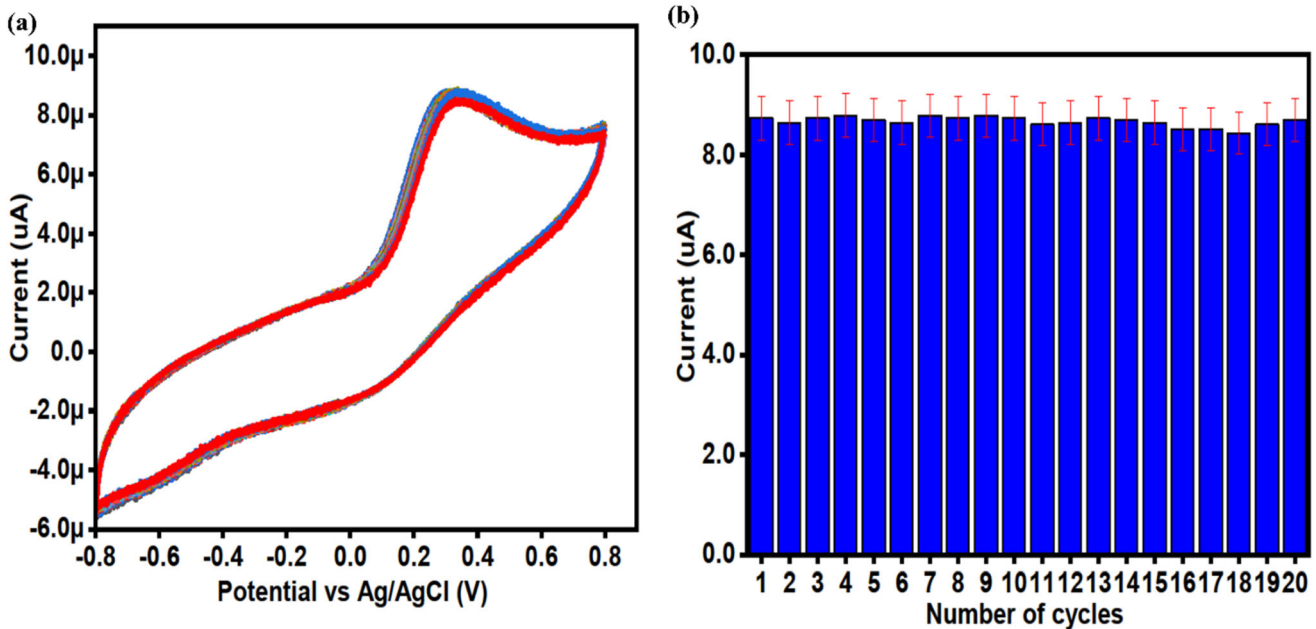


Fig. 13 a Cyclic voltammograms at a scan rate of 50 mV/s of MGCE with 10 mL of garlic leaves extract assisted NiCo₂O₄ in the presence of 0.5 mM AA in 0.1 M PBS pH 7.4. **b** bar graph of peak

current for the description of change in the peak current with increasing number of CV cycles. Linear plot of peak current versus successive increase of AA concentrations

approach has excellent analytical properties and that NiCo_2O_4 nanostructures are suitable for long-term applications. The amperometric response of NiCo_2O_4 nanostructures in a 0.5 mM AA solution was measured over a period of 1000 s to determine the stability of these nanostructures. Amperometry results can be seen in Fig. 14a. In view of the fact that there was no current fluctuation during testing, it can be concluded that the current AA sensor is adequate for long-term use. Compared to other reported AA sensors/biosensors in the literature, the sensor/biosensor was improved due to its wide linear range, low detection limit, and low fabrication cost. With a sweeping frequency range of 100 kHz to 1 Hz, an amplitude of 10 mV, and a bias potential of 0.4 V, we conducted electrochemical impedance spectroscopy (EIS) on NiCo_2O_4 nanostructures in order to improve electrochemical performance. For three NiCo_2O_4 nanostructures, including the virgin sample, sample 1 and sample 2 in 0.5 mM AA, Nyquist plots were measured. As indicated by the Nyquist plots of sample 2, the low arc indicates a fast charge transfer between the NiCo_2O_4 nanostructured working electrode and analyte solution at 0.5 mM, whereas the intercept at high frequency indicates the resistance of the electrolyte [47]. It is evident from Nyquist plots

that the pristine NiCo_2O_4 nanostructures, samples 1 and 3, are limited by poor charge transfer.

3.4 Method of preparation real sample and their analysis

For practical applications, it is essential to examine the electrode's performance during the analysis of real samples. Commercial orange juice was purchased from a nearby market (in Sindh, Pakistan) and tested to validate the sensor's practical application for AA detection. Several filters were needed to remove suspended particles and pulp from the sample. A 25 mL solution of PBS at a pH of 7.4 was added to 10 mL of filtered juice. In Table 2, the results are presented. A standard recovery method was used to confirm the results. As a method of determining AA levels in real samples, ce-cone chewable tablets, which contain vitamin C, were selected. Chewable ce-cone tablets were obtained from a nearby pharmacy. A mixture of crushed vitamin C chewable pills (500 mg/tablet) was mixed with 10.0 mL of PBS 0.1 M, pH 7.4. The mixture was centrifuged for 20 min at 13,000 rpm. 100 mL of supernatant was diluted to 10.0 mL of ultrapure water to prepare the stock solution for the vitamin C chewable pills. AA content of Ce-cone tablet stock solution was

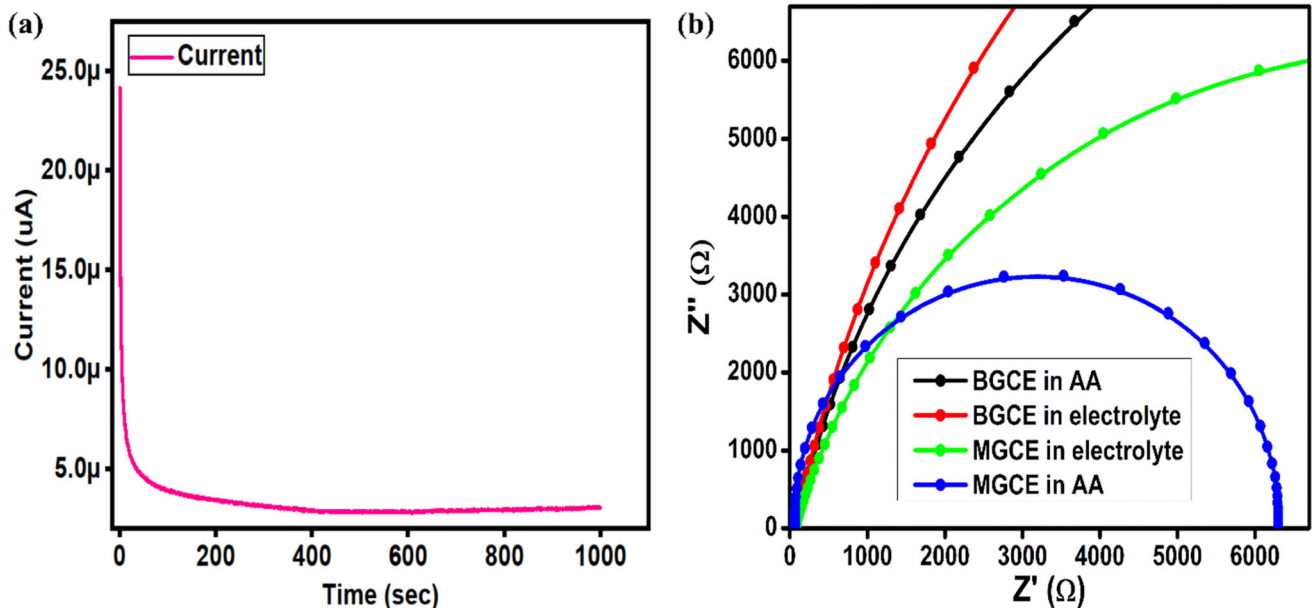


Fig. 14 a Chronoamperometric response of MGCE with 10 mL of garlic extract assisted NiCo_2O_4 in 0.5 mM prepared in 0.1 M PBS pH 7.4 for the demonstration of stability of modified electrode, b EIS Nyquist plots collected for the MGCE with and 10 mL of

garlic extract assisted NiCo_2O_4 in 0.5 mM AA using frequency range of 100 kHz to 1 Hz, amplitude of 10 mV and biasing potential of 0.6 V

Table 2 Practical performance of NiCo₂O₄ prepared with 10 mL of garlic leaves extract using standard addition method by following (%) recovery method

Sample ID	Added (mM)	Found (mM)	Recovery (%)	RSD (%)
Commercial orange juice	0.5	0.523 ± 0.0051	105	0.541
	1	1.494 ± 0.0065	100	0.492
	1.5	3.082 ± 0.0071	103	0.523
Ce-cone tablet	0.5	0.513 ± 0.0082	103	0.513
	1	1.521 ± 0.0048	101	0.484
	1.5	3.062 ± 0.0061	102	0.535

determined using the standard addition method, and recoveries were calculated to assess the method's accuracy. NiCo₂O₄ nanostructures prepared with 10 mL garlic leaves extract provided highly encouraging results for the potential application of NiCo₂O₄ nanostructures for AA detection. Due to the high density of active sites present on garlic leaves, their surface properties have changed. A high electrode compatibility of NiCo₂O₄ nanostructures allows them to exhibit excellent sensing performance by promoting charge transfer at the interface.

4 Conclusions

Nanostructures of NiCo₂O₄ were synthesized from garlic leaf extract by hydrothermal synthesis. To develop optimized electroactive materials based on NiCo₂O₄ nanostructures, various amounts of garlic juice, including 5 mL, 10 mL, and 15 mL were used. Analyses have been conducted on the shape, crystal quality, surface chemical composition, and elemental composition of the material. A garlic leaf extract exhibited phytochemical properties such as reducing, capping, and stabilizing agents, which strongly altered NiCo₂O₄ surface properties. In a non-enzymatic approach, the optimized NiCo₂O₄ nanostructures were found to be highly sensitive to AA detection using 10 mL garlic leaf extract. An AA sensor with a linear range of 0.5 mM to 8.5 mM and a detection limit of 0.01 mM is presented. In this study, AA sensors were tested for stability, repeatability, and selectivity. Since garlic leaves are biomass waste, they can be used to prepare highly electroactive materials for use in energy conversion, storage, and medicine.

Acknowledgements

The authors would like to gratefully acknowledge the Higher Education Commission Pakistan for partial support under the Project NRPU/8350. We also extend our sincere appreciation to the Researchers Supporting Project Number (RSP2023R79) at King Saud University, Riyadh, Saudi Arabia. Brigitte Vigolo would like to thank the platform "Microscopies, Microprobes and Metallography (3 M)" (Institut Jean Lamour, IJL, Nancy, France) for access to SEM facilities and F. Alnjiman for his valuable help. Authors would also like to acknowledge partial funding of the Ajman University, Grant ID: DRGS ref. 2022-IRG-HBS-5.

Author contribution

AGS, did the material synthesis and evaluate the preliminary sensor performance. AT, did the XRD and analyzed the results. ASC, did in depth sensor performance of as prepared materials. TP, did the partial supervision. ZAS, did the EDS analysis and preview the draft of manuscript. FC, did the EIS analysis. MAB, did the SEM analysis. ALB, did real sample analysis. SK, analyzed the electroanalytical results. AH, did TEM and HRTEM analysis. ED, did the editing of draft and preview of the analyzed results. AAKHI, did plausible growth mechanism and edited the revised draft of manuscript. SSM, did mechanism analysis based CV data. AN, did proofreading and validate the electrochemical results. LVK, did HRTEM and XPS measurements. BV, did XPS analysis and proofread the paper. ZHI, did main supervision, wrote the first draft and preview obtained results.

Data availability

Data sets generated during the current study are available from the corresponding author on reasonable request.

Declarations

Conflict of interest Authors declare no competing interests in the resented research work.

References

- M. Li, S. Zhang, H. Li, M. Chen, Cerium/polyacrylic acid modified porphyrin metal-organic framework as fluorescence and photothermal sensor for ascorbic acid measurement. *Talanta* **252**, 123825 (2023)
- W.S. Kim, R.L. Dahlgren, L.L. Moroz, J.V. Sweedler, Ascorbic acid assays of individual neurons and neuronal tissues using capillary electrophoresis with laser-induced fluorescence detection. *Anal. Chem.* **74**, 5614 (2002)
- S.E. Bohndiek, M.I. Kettunen, D.E. Hu, B.W. Kennedy, J. Boren, F.A. Gallagher, M. Brindle, Hyperpolarized [1-¹³C]-ascorbic and dehydroascorbic acid: vitamin C as a probe for imaging redox status in vivo. *J. Am. Chem. Soc.* **133**, 11795 (2011)
- X. Luo, W. Zhang, Y. Han, X. Chen, L. Zhu, W. Tang, J. Wang, T. Yue, Z. Li, N, S co-doped carbon dots based fluorescent “on-off-on” sensor for determination of ascorbic acid in common fruits. *Food Chem.* **258**, 214 (2018)
- R. Liu, R. Yang, C. Qu, H. Mao, Y. Hu, J. Li, L. Qu, Synthesis of glycine-functionalized graphene quantum dots as highly sensitive and selective fluorescent sensor of ascorbic acid in human serum. *Sens. Actuators B Chem.* **241**, 644 (2017)
- V. Valdramidis, P.J. Cullen, B. Tiwari, C.P. O'Donnell, Quantitative modelling approaches for ascorbic acid degradation and non-enzymatic browning of orange juice during ultrasound processing. *J. Food Eng.* **96**, 449 (2010)
- M. Noroozifar, M. Khorasani-Motlagh, Solid-phase iodine as an oxidant in flow injection analysis: determination of ascorbic acid in pharmaceuticals and foods by background correction. *Talanta* **61**, 173 (2003)
- A. Jain, A. Chaurasia, K.K. Verma, Determination of ascorbic acid in soft drinks, preserved fruit juices and pharmaceuticals by flow injection spectrophotometry: matrix absorbance correction by treatment with sodium hydroxide. *Talanta* **42**, 779 (1995)
- S. Arya, M. Mahajan, P. Jain, Non-spectrophotometric methods for the determination of vitamin C. *Anal. Chim. Acta* **417**, 1 (2000)
- Y. Tang, M. Wu, A quick method for the simultaneous determination of ascorbic acid and sorbic acid in fruit juices by capillary zone electrophoresis. *Talanta* **65**, 794 (2005)
- T. Perez-Ruiz, C. Martinez-Lozano, V. Tomas, J. Fenol, Fluorimetric determination of total ascorbic acid by a stopped-flow mixing technique. *Analyst* **126**, 1436 (2001)
- M. Bijad, H. Karimi-Maleh, M.A. Khalilzadeh, Application of ZnO/CNTs nanocomposite ionic liquid paste electrode as a sensitive voltammetric sensor for determination of ascorbic acid in food samples. *Food Anal. Methods* **6**, 1639 (2013)
- L.A. Pachla, P.T. Kissinger, Determination of ascorbic acid in foodstuffs, pharmaceuticals, and body fluids by liquid chromatography with electrochemical detection. *Anal. Chem.* **48**, 364 (1976)
- J. Lykkesfeldt, Determination of ascorbic acid and dehydroascorbic acid in biological samples by high-performance liquid chromatography using subtraction methods: reliable reduction with tris [2-carboxyethyl] phosphine hydrochloride. *Anal. Biochem.* **282**, 89 (2000)
- R. Sha, S. Badhulika, Facile green synthesis of reduced graphene oxide/tin oxide composite for highly selective and ultra-sensitive detection of ascorbic acid. *J. Electroanal. Chem.* **816**, 30 (2018)
- A. Özcan, Y. Şahin, Preparation of selective and sensitive electrochemically treated pencil graphite electrodes for the determination of uric acid in urine and blood serum. *Biosens. Bioelectron.* **25**, 2497 (2010)
- M.B. Wayu, M.A. Schwarzmann, S.D. Gillespie, M.C. Leopold, Enzyme-free uric acid electrochemical sensors using β -cyclodextrin-modified carboxylic acid-functionalized carbon nanotubes. *J. Mater. Sci.* **52**, 6050 (2017)
- J. Wang, B. Yang, J. Zhong, Dopamine and uric acid electrochemical sensor based on a glassy carbon electrode modified with cubic Pd and reduced graphene oxide nanocomposite. *J. Colloid Interface Sci.* **497**, 172–180 (2017)
- R. Ding, L. Qi, M. Jia, H. Wang, Facile synthesis of mesoporous spinel NiCo₂O₄ nanostructures as highly efficient electrocatalysts for urea electro-oxidation. *Nanoscale* **6**, 1369 (2014)
- G. Zhang, T. Wang, X. Yu, H. Zhang, H. Duan, B. Lu, Nanoforest of hierarchical Co₃O₄@NiCo₂O₄ nanowire arrays for high-performance supercapacitors. *Nano Energy* **2**, 586 (2013)
- E. Jokar, A.I. Zad, S. Shahrokhian, Synthesis and characterization of NiCo₂O₄ nanorods for preparation of supercapacitor electrodes. *J. Solid State Electrochem.* **19**, 269 (2015)

22. G. Huang, L. Zhang, F. Zhang, L. Wang, Metal–organic framework derived $\text{Fe}_2\text{O}_3@\text{NiCo}_2\text{O}_4$ porous nanocages as anode materials for Li-ion batteries. *Nanoscale* **6**, 5509 (2014)
23. Q. He, J. Liu, X. Liu, D. Chen, P. Deng, J. Liang, Fabrication of amine-modified magnetite-electrochemically reduced graphene oxide nanocomposite modified glassy carbon electrode for sensitive dopamine determination. *Nanomaterials* **8**, 194 (2018)
24. Y. Zhou, L. Ma, M. Gan, M. Ye, X. Li, Y. Zhai, F. Yan, F. Cao, Monodisperse $\text{MnO}_2@\text{NiCo}_2\text{O}_4$ core/shell nanospheres with highly opened structures as electrode materials for good-performance supercapacitors. *Appl. Surf. Sci.* **444**, 1 (2018)
25. K. Xu, X. Yang, J. Yang, J. Hu, Synthesis of hierarchical $\text{Co}_3\text{O}_4@\text{NiCo}_2\text{O}_4$ core-shell nanosheets as electrode materials for supercapacitor application. *J. Alloy. Compd.* **700**, 247 (2017)
26. Q. Chu, B. Yang, W. Wang, W. Tong, X. Wang, X. Liu, J. Chen, Fabrication of a stainless-steel-mesh-supported hierarchical $\text{Fe}_2\text{O}_3@\text{NiCo}_2\text{O}_4$ core-shell tubular array anode for lithium-ion battery. *ChemistrySelect* **1**, 5569 (2016)
27. S. Kumar, A. Tahira, A.L. Bhatti, M.A. Bhatti, R.H. Mari, N.M. Shaikh, M.Y. Solangi, A. Nafady, M. Emo, B. Vigolo, A.I. Molina, A. Vomiero, Z.H. Ibupoto, Transforming NiCo_2O_4 nanorods into nanoparticles using citrus lemon juice enhancing electrochemical properties for asymmetric supercapacitor and water oxidation. *RSC Adv.* **13**, 18614 (2023)
28. H. Nawaz, M.A. Shad, A. Rauf, Optimization of extraction yield and antioxidant properties of *Brassica oleracea Convar capitata* var. L. leaf extracts. *Food Chem.* **242**, 182 (2018)
29. S. Amin, A. Tahira, A.R. Solangi, R. Mazzaro, Z.H. Ibupoto, A. Fatima, A. Vomiero, Functional nickel oxide nanostructures for ethanol oxidation in alkaline media. *Electroanalysis* **32**, 1052 (2020)
30. A. Hanan, M. Ahmed, M.N. Lakhan, A.H. Shar, D. Cao, A. Asif, A. Ali, M. Gul, Novel $\text{rGO}@\text{Fe}_3\text{O}_4$ nanostructures: an active electrocatalyst for hydrogen evolution reaction in alkaline media. *J. Indian Chem. Soc.* **99**, 100442 (2022)
31. M. Gong, W. Zhou, M.C. Tsai, J. Zhou, M. Guan, M.C. Lin, B. Zhang, Y. Hu, D.Y. Wang, J. Yang, S.J. Pennycook, Nanoscale nickel oxide/nickel heterostructures for active hydrogen evolution electrocatalysis. *Nat. Commun.* **5**, 4695 (2014)
32. T.H. Lim, S.J. Cho, H.S. Yang, M.H. Engelhard, D.H. Kim, Effect of Co/Ni ratios in cobalt nickel mixed oxide catalysts on methane combustion. *Appl. Catal. A* **505**, 62 (2015)
33. M.T. Ahsan, M. Usman, Z. Ali, S. Javed, R. Ali, M.U. Farooq, M.A. Akram, A. Mahmood, 3D hierarchically mesoporous zinc-nickel-cobalt ternary oxide ($\text{Zn}_{0.6}\text{Ni}_{0.8}\text{Co}_{1.6}\text{O}_4$) nanowires for high-performance asymmetric supercapacitors. *Front. Chem.* **8**, 487 (2020)
34. H. Li, C. Cai, Q. Wang, S. Chen, J. Fu, B. Liu, Q. Hu, K. Hu, H. Li, J. Hu, Q. Liu, High-performance alkaline water splitting by Ni nanoparticle-decorated Mo-Ni microrods: Enhanced ion adsorption by the local electric field. *Chem. Eng. J.* **435**, 134860 (2022)
35. A. Hanan, D. Shu, U. Aftab, D. Cao, A.J. Laghari, M.Y. Solangi, M.I. Abro, A. Nafady, B. Vigolo, A. Tahira, Z.H. Ibupoto, $\text{Co}_2\text{FeO}_4@\text{rGO}$ composite: Towards trifunctional water splitting in alkaline media. *Int. J. Hydrogen Energy* **47**, 33919 (2022)
36. W. Li, B. Zhang, R. Lin et al., A dendritic nickel cobalt sulfide nanostructure for alkaline battery electrodes. *Adv. Funct. Mater.* **28**, 1705937 (2018)
37. J. López-Tinoco, R. Mendoza-Cruz, L. Bazán-Díaz et al., The preparation and characterization of Co–Ni nanoparticles and the testing of a heterogenized Co–Ni/alumina catalyst for CO hydrogenation. *Catalysts* **10**, 18 (2019)
38. N. Wang, T. Hang, D. Chu, M. Li, Three-dimensional hierarchical nanostructured Cu/Ni–Co coating electrode for hydrogen evolution reaction in alkaline media. *Nano-micro Lett.* **7**, 347 (2015)
39. Y. Lei, J. Li, Y. Wang et al., Rapid microwave-assisted green synthesis of 3D hierarchical flower-shaped NiCo_2O_4 microsphere for high-performance supercapacitor. *ACS Appl. Mater. Interfaces.* **6**, 1773 (2014)
40. J. Marco, J. Gancedo, M. Gracia, J. Gautier, E. Ríos, F. Berry, Characterization of the nickel cobaltite, NiCo_2O_4 , prepared by several methods: an XRD, XANES, EXAFS, and XPS study. *J. Solid State Chem.* **153**, 74 (2000)
41. H. Guan, B. Peng, D. Gong, B. Han, N. Zhang, Electrochemical enhanced detection of uric acid based on peroxidase-like activity of $\text{Fe}_3\text{O}_4@\text{Au}$. *Electroanalysis* **33**, 1736 (2021)
42. Z. Hassanvand, F. Jalali, Simultaneous determination of l-DOPA, l-tyrosine and uric acid by cysteine acid-modified glassy carbon electrode. *Mater. Sci. Eng. C* **98**, 496 (2019)
43. J. Lv, C. Li, S. Feng et al., A novel electrochemical sensor for uric acid detection based on PCN/MWCNT. *Ionics* **25**, 4437 (2019)
44. L. Ma, Q. Zhang, C. Wu, Y. Zhang, L. Zeng, PtNi bimetallic nanoparticles loaded MoS_2 nanosheets: preparation and electrochemical sensing application for the detection of dopamine and uric acid. *Anal. Chim. Acta* **1055**, 17 (2019)
45. N.G. Tsierekzos, U. Ritter, Y.N. Thaha, C. Downing, P. Szroeder, P. Scharff, Multi-walled carbon nanotubes doped with boron as an electrode material for electrochemical studies on dopamine, uric acid, and ascorbic acid. *Microchim. Acta* **183**, 35 (2016)
46. C. Wang, J. Du, H. Wang et al., A facile electrochemical sensor based on reduced graphene oxide and Au nanoplates

- modified glassy carbon electrode for simultaneous detection of ascorbic acid, dopamine and uric acid. *Sens. Actuators B Chem.* **204**, 302 (2014)
47. Y.Q. Wu, X.Y. Chen, P.T. Ji, Q.Q. Zhou, Sol-gel approach for controllable synthesis and electrochemical properties of NiCo_2O_4 crystals as electrode materials for application in supercapacitors. *Electrochim. Acta* **56**, 7517 (2011)
48. A. Kumar, V.L. Furtado, J.M. Gonçalves et al., Amperometric microsensor based on nanoporous gold for ascorbic acid detection in highly acidic biological extracts. *Anal. Chim. Acta* **1095**, 61 (2020)
49. C. Manjunatha, V. Chirag, B.W. Shivaraj, N. Srinivasa, S. Ashoka, One pot green synthesis of novel $\text{rGO}@ZnO$ nanocomposite and fabrication of electrochemical sensor for ascorbic acid using screen-printed electrode. *J. Nanostruct.* **10**, 531 (2020)
50. Z. Ce, J. Zhong, S. Li et al., Fabrication of reduced graphene oxide-bimetallic PdAu nanocomposites for the electrochemical determination of ascorbic acid, dopamine, uric acid and rutin. *J. Electroanal. Chem.* **805**, 110 (2017)
51. A. Abellán-Llobregat, L. Vidal, R. Rodríguez-Amaro, A. Canals, E. Morallon, Evaluation of herringbone carbon nanotubes-modified electrodes for the simultaneous determination of ascorbic acid and uric acid. *Electrochim. Acta* **285**, 284 (2018)
52. D. Ji, Z. Liu, L. Liu et al., Smartphone-based integrated voltammetry system for simultaneous detection of ascorbic acid, dopamine, and uric acid with graphene and gold nanoparticles modified screen-printed electrodes. *Biosens. Bioelectron.* **119**, 55 (2018)
53. T. Sathesh Babu, D. Varadarajan, G. Murugan, T. Ramachandran, B.G. Nair, Gold nanoparticle-polypyrrole composite modified TiO_2 nanotube array electrode for the amperometric sensing of ascorbic acid. *J. Appl. Electrochem.* **42**, 427 (2012)
54. Y. Chu, H. Zhou, X. Wang et al., A flexible and self-supported nanoporous gold wire electrode with a seamless structure for electrochemical ascorbic acid sensor. *Microchem. J.* **186**, 108259 (2023)
55. L. Xi, D. Ren, J. Luo, Y. Zhu, Electrochemical analysis of ascorbic acid using copper nanoparticles/polyaniline modified glassy carbon electrode. *J. Electroanal. Chem.* **650**, 127 (2010)
56. K. Ghanbari, N. Hajheidari, $\text{ZnO-Cu}_2\text{O}$ /polypyrrole nanocomposite modified electrode for simultaneous determination of ascorbic acid, dopamine, and uric acid. *Anal. Biochem.* **473**, 53 (2015)
57. M. Wang, M. Cui, W. Liu, X. Liu, Highly dispersed conductive polypyrrole hydrogels as sensitive sensor for simultaneous determination of ascorbic acid, dopamine and uric acid. *J. Electroanal. Chem.* **832**, 174 (2019)
58. L. Shao, X. Wang, B. Yang et al., A highly sensitive ascorbic acid sensor based on hierarchical polyaniline coated halloysite nanotubes prepared by electrophoretic deposition. *Electrochim. Acta* **255**, 286 (2017)
59. Y. Shen, L. Zheng, Polyaniline-poly (methylene blue) nanorod composites as an electrochemical sensor for sensitive determination of ascorbic acid. *Int. J. Electrochem. Sci.* **18**, 6 (2023)
60. N. Tukimin, J. Abdullah, Y. Sulaiman, Electrodeposition of poly (3, 4-ethylenedioxythiophene)/reduced graphene oxide/manganese dioxide for simultaneous detection of uric acid, dopamine and ascorbic acid. *J. Electroanal. Chem.* **820**, 74 (2018)
61. A.S. Chang, A. Tahira, F. Chang et al., Highly heterogeneous morphology of cobalt oxide nanostructures for the development of sensitive and selective ascorbic acid non-enzymatic sensor. *Biosensors* **13**, 147 (2023)
62. B. Habibi, M.H. Pournaghi-Azar, Simultaneous determination of ascorbic acid, dopamine and uric acid by use of a MWCNT modified carbon-ceramic electrode and differential pulse voltammetry. *Electrochim. Acta* **55**, 5492 (2010)
63. D. Zheng, J. Ye, L. Zhou, Y. Zhang, C. Yu, Simultaneous determination of dopamine, ascorbic acid and uric acid on ordered mesoporous carbon/Nafion composite film. *J. Electroanal. Chem.* **625**, 82 (2009)
64. A. Jo, M. Kang, A. Cha et al., Nonenzymatic amperometric sensor for ascorbic acid based on hollow gold/ruthenium nanoshells. *Anal. Chim. Acta* **819**, 94 (2014)
65. D. Han, T. Han, C. Shan, A. Ivaska, L. Niu, Simultaneous determination of ascorbic acid, dopamine and uric acid with chitosan-graphene modified electrode. *Electroanalysis* **22**, 2001 (2010)

Publisher's Note Springer Nature remains neutral with regard to jurisdictional claims in published maps and institutional affiliations.

Springer Nature or its licensor (e.g. a society or other partner) holds exclusive rights to this article under a publishing agreement with the author(s) or other rightsholder(s); author self-archiving of the accepted manuscript version of this article is solely governed by the terms of such publishing agreement and applicable law.